JOURNAL OF MATERIALS SCIENCE 31 (1996) 4617–4624

Perovskite-type $BaTiO_3$ ceramics containing particulate SiC

Part I *Structure variation and phase transformation*

H.J. HWANG, T. SEKINO, K. OTA, K. NIIHARA
The Institute of Scientific and Industrial Research, Osaka University, 8-1 Mihogaoka, Ibaraki, Osaka 567, Japan

$BaTiO_3$-based composites with nanosized SiC particulates were successfully fabricated by a hot-pressing technique in an argon atmosphere. Crystal structure and phase transformation behaviour were investigated by X-ray diffraction analysis, linear thermal expansion analysis and internal friction measurement. It was confirmed that the added SiC particulates were uniformly distributed within the matrix $BaTiO_3$ grains, with some larger particulates located at the $BaTiO_3$ grain boundaries. In addition, there were no reaction phases between $BaTiO_3$ matrix and SiC particulates. The crystal structure gradually changed from tetragonal to cubic phase with respect to the SiC content. The Curie temperature, T_c, was lowered as the SiC content increased. Moreover, the transformations in the low-temperature range almost disappeared above 1 vol % SiC. The diffused phase transformation phenomenon was observed as the SiC content increased up to 3 vol %. The results were associated with the grain-size reduction, the existence of oxygen vacancies and the residual stresses associated with the thermal expansion mismatch between matrix and SiC particulate. The influence on the domain structure development of SiC particulates dispersed within the matrix grains was also discussed.

1. Introduction

The perovskite structure-type ceramics $BaTiO_3$ are widely used for positive temperature coefficient (PTC) thermistors, capacitors of high-dielectric constant, gas sensor and other electronic devices. Their electrical/dielectric properties and grain-boundary structure, including the PTCR (positive temperature coefficient of resistivity) phenomenon, have been studied extensively [1–3]. It is well known that characteristics of the perovskite-type ceramics are markedly affected by their crystal structure and microstructure, which are dependent upon the fabrication processes such as the powder preparation technique and sintering conditions as well as the kind, amount and properties of dopants [4]. Furthermore, the dielectric and mechanical strength, in particular, are very sensitive to the structural variation and phase transformation behaviour [5].

In the area of microstructural development, approaches for the microstructural modification in $BaTiO_3$-based ceramics can be largely classified into three categories. First is a compositional modification [6–8]. The characteristics of $BaTiO_3$-based ceramics can be altered by the substitution of equivalent atoms for barium and titanium sites [6]. $BaTiO_3$ ceramics fabricated by these compositional modifications have different crystal structures and Curie temperatures. In addition, a wide variety of heterovalent ions can be substituted at barium or titanium sites independently or at both sites simultaneously. In these cases, semiconducting $BaTiO_3$ ceramics can be obtained by adding a small amount of dopants, so that it is possible to fabricate the PTC thermistor and grain-boundary barrier layer (GBBL) capacitor. The second category is the modification by introducing oxide additives into $BaTiO_3$-based ceramics [9]. Oxide additives forming liquid phases at low temperatures change the microstructure, including the grain-boundary structure, and also improve the sinterability. Finally, the core–shell structure, in which ferroelectric and paraelectric phases coexisted, was also reported [10, 11].

On the other hand, there are only a few studies about the particulate-dispersed $BaTiO_3$-based composite [12, 13]. This is caused by the fact that the reactivity between $BaTiO_3$ and particulate additives used is relatively high enough to form a solid solution and/or unwanted reaction phases. Only limited kinds of materials can be employed as a secondary particulate for $BaTiO_3$-based ceramics. Emoto and Hojo [12] reported the fabrication process and dielectric properties of $BaTiO_3$-Ni composite.

In the present study, new types of $BaTiO_3$-based composites, containing nanosized SiC particulate as a secondary phase, were fabricated. Crystal structural variation and perovskite-type transformation

0022–2461

behaviour were investigated in detail. It is well known that SiC plays an important role as a grain-boundary controller as well as a microstructure modifier in various fields of ceramic systems [14, 15]. Moreover, it is expected that the reactivity between $BaTiO_3$ and SiC is not too high to form a solid solution with each other or any kind of unwanted compounds. The main emphasis was placed on an understanding of the relationship between the phase transformation behaviour and microstructure for the dense and fine-grained $BaTiO_3$ with nanosized SiC particulate.

2. Experimental procedure

2.1. Material preparation

Monolithic $BaTiO_3$ and $BaTiO_3$-based composites with SiC particulates were prepared using a conventional powder metallurgical method. The starting materials were $BaTiO_3$ (Sakai Chemical Industry Co. Ltd, Osaka, Japan) and β-SiC (Mitsui Toatsu Chemical Co. Ltd, Tokyo, Japan) powders with average particle sizes of 0.1 and 0.07 μm, respectively. The crystal phase of the starting $BaTiO_3$ powder was cubic and the Ba/Ti atomic ratio was 0.999. The purity and some physical properties of $BaTiO_3$ and β-SiC powders are shown in Tables I and II. The amount of SiC was varied from 0.2–10 vol % in $BaTiO_3$. $BaTiO_3$ powder with the required amount of SiC was wet ball-milled in ethyl alcohol using a polyethylene pot and ZrO_2 balls for 24 h. The wet milled slurry was then dried. Dried powder was milled again and sieved through a 320 μm mesh screen. The mixed powders were hot pressed at 1100–1400 °C under a pressure of 30 MPa for 1 h in an argon atmosphere. The heating rate was 15 °C min^{-1}. Sintered specimens were cut with a diamond saw. The section surface was polished with diamond pastes for various evaluations and observations, as will be mentioned later.

TABLE I Characterization and chemical analysis of $BaTiO_3$ powder used in the present study

Average particle size (μm)[a]		0.1
Specific surface area ($m^2 g^{-1}$)		11.4
Purity (wt %) :		
	Ba/Ti (atomic ratio)	0.999
	SrO	0.01
	CaO	0.001
	Na_2O	0.003
	SiO_2	0.005
	Al_2O_3	0.001
	Fe_2O_3	0.003

[a] SEM observation.

TABLE II Characterization and chemical analysis of SiC powder used in the present study

Average particle size (μm)[a]		0.07
Specific surface area ($m^2 g^{-1}$)		18.2
Purity (p.p.m.) :		
	Free-SiO_2 (wt %)	0.12
	Fe	190
	Ni	20
	Cr	70
	Ca	20
	Al	30

[a] TEM observation.

2.2. Characterization

The bulk density was determined by Archimedes' method in toluene. The X-ray diffraction (XRD) pattern was taken using nickel-filtered CuK_α radiation. The grain size of the specimens was determined from scanning electron micrographs of etched surfaces using a linear intercept method [16]. The average linear intercept, L, was measured, and then L ($\pi/2$) was taken to be an average grain size, G. Fracture surfaces and domain structure were observed with a scanning electron microscope (SEM) and a transmission electron microscope (TEM), respectively.

The linear thermal expansion was measured using a thermo-dilatometric analyser on rectangular test specimens of $3 \times 4 \times 20$ mm^3. The internal friction was measured at frequencies ranging from 1–20 Hz from −196 to 200 °C in nitrogen by an inverted torsion pendulum method. Specimens were $4 \times 2 \times 45$ mm^3 in dimension. Measurements were made automatically on both heating and cooling runs at each 2 °C interval. The vibration amplitude was detected by the eddy current induced in a displacement meter placed close to the pendulum. In order to measure the carrier concentration, Hall measurements were performed at room and liquid nitrogen temperatures using the Van Der Pauw method with rectangular specimens (10×10 mm^2) in a magnetic field of about 3000 G [17]. Before the Hall measurements, indium/gallium alloy electrodes, which are ohmic for n-type semiconductors, were baked on one side of the specimen at 350 °C for 30 min to diffuse sufficiently into the specimen.

3. Results

X-ray diffraction analysis showed that the monolithic $BaTiO_3$ was tetragonal phase, regardless of the sintering temperature. $BaTiO_3$-based composites sintered at 1300 °C were mainly composed of $BaTiO_3$ and β-SiC. The SiC addition up to 5 vol % gave no additional phases such as $Ba_4Ti_{13}O_{30}$, $Ba_6Ti_{17}O_{30}$, and $BaTiO_3$–xBaO compounds. A small amount of $Ba_2TiSi_2O_8$ phase started to appear in the $BaTiO_3$ –5 vol % SiC composite sintered above 1300 °C. The formation of $Ba_2TiSi_2O_8$ phase is due to the reaction between $BaTiO_3$ and SiO_2 which is present in the starting $BaTiO_3$ and/or β-SiC powders, as can be seen in Tables I and II.

The relative density of monolithic $BaTiO_3$ increased monotonously with increasing sintering temperature. Nearly full density was achieved for the monolithic $BaTiO_3$ hot pressed at 1200 °C. The incorporation of the SiC particulate, however, lowered tremendously the densification rate. A high relative density (99% theoretical density) could be obtained for $BaTiO_3$ with 1 vol % SiC when the sintering temperature was raised to 1300 °C. As the SiC content increased, the maximum relative density was lowered to 97% and 96% for $BaTiO_3$–3 vol % SiC and

5 vol % SiC composites sintered at 1300 °C, respectively. Even though the sintering temperature was raised to 1350 or 1400 °C, no remarkable relative density change was observed.

From TEM observations, most of the SiC particulates were uniformly distributed within the matrix $BaTiO_3$ grains, with some larger particulates located at the $BaTiO_3$ grain boundaries. In addition, no reaction phases were observed between $BaTiO_3$ matrix and SiC particulates incorporated within $BaTiO_3$ matrix grains, nor at matrix grain boundaries and/or three-grain junctions.

Typical high-angle X-ray diffraction profiles between 107° and 111°, and 139° and 143° in the 2θ range for monolithic $BaTiO_3$ and $BaTiO_3$–SiC composites are shown in Fig. 1a and b. The incorporation of the SiC particulate has a remarkable effect on the crystal structure change. In general, it is well known that the group of reflection planes of (1 1 4), (4 1 1), and (2 2 4), (4 2 2) is very sensitive to the crystal structural variation of $BaTiO_3$, even when its amount is extremely small. The cubic structure gives a set of doublets formed by reflections from the same phase of the two wavelengths K_{α_1} and K_{α_2}, whereas, in the tetragonal structure each doublet is split into a set of partly overlapping doublets [18]. It is evident from the high-angle X-ray diffraction profiles that characteristic peaks of tetragonal structure are still present up to 1 vol % SiC addition. Over 3 vol % SiC addition, however, it is nearly impossible to identify the crystal planes of (1 1 4) and (2 2 4) from (4 1 1) and (4 2 2), respectively. These results suggest that the crystal structure of $BaTiO_3$–SiC composites with more than 1 vol % is pseudo-cubic phase, not tetragonal phase.

Fig. 2 shows the linear thermal expansion curves, $\Delta L/L_0$ (where L_0 is the length of the specimen at 20 °C) for specimens sintered at 1300 °C. For the monolithic $BaTiO_3$, the tetragonal to cubic transformation was clearly observed at about 110 °C. This transformation temperature is lower than that observed for pure $BaTiO_3$ ceramics sintered in an air atmosphere. The sintering in a reducing atmosphere results in crystal structural disorder arising from oxygen vacancies [19]. For all the specimens, it is suggested that there are greater extents of deviation from the typical perovskite structure [20]. T_c decreased monotonously as the SiC content increased up to 1 vol %. When the SiC content was more than 3 vol %, T_c became ambiguous and broadened in the wide temperature range 30–80 °C. In order to investigate the effects of the oxygen vacancy on the crystal structure and the phase transformation behaviour of $BaTiO_3$–SiC composites, the heating curves for $\Delta L/L_0$ of specimens sintered at 1300 °C in an argon atmosphere and subsequently oxidized at 1050 °C for 30 min, are shown in Fig. 3. All the $\Delta L/L_0$ curves were largely changed compared with those observed in Fig. 2, and T_c also returned to near 120 °C.

The transformation behaviour in the low temperature range (− 196 to 200 °C) was evaluated by internal friction measurement. Fig. 4 shows internal friction curves with respect to the temperature in the range − 196 to 200 °C for specimens sintered at 1300 °C in an argon atmosphere. When the transformation occurred in the perovskite-type ceramics, energy relaxation resulting from atomic movements towards the lower energy state, might occur. In the present study, internal friction curves increase rapidly at the temperature corresponding to the perovskite transformation temperature for composites with less than 1 vol % SiC. It is believed that the monolithic $BaTiO_3$ and $BaTiO_3$–0.2 vol % SiC composite exhibit typical cubic-to-tetragonal transformations at around 120 °C,

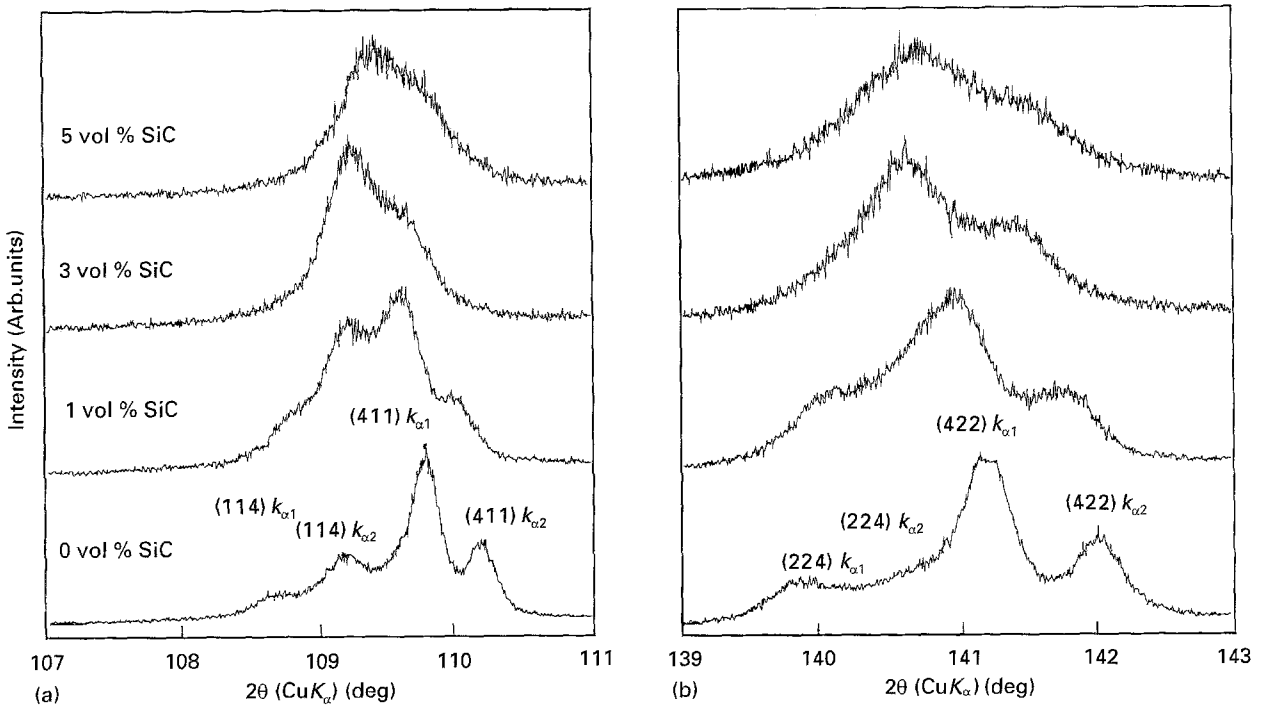

Figure 1 High-angle X-ray diffraction profiles for the monolithic $BaTiO_3$ and $BaTiO_3$–1 vol %, 3 vol %, and 5 vol % SiC composites sintered at 1300 °C for 1 h in an argon atmosphere.

tetragonal-to-orthorhombic at around 0 °C and orthorhombic-to-rhombohedral at around −100 °C, respectively. Accordingly it is evident that the perovskite structure remains for the monolithic $BaTiO_3$ and

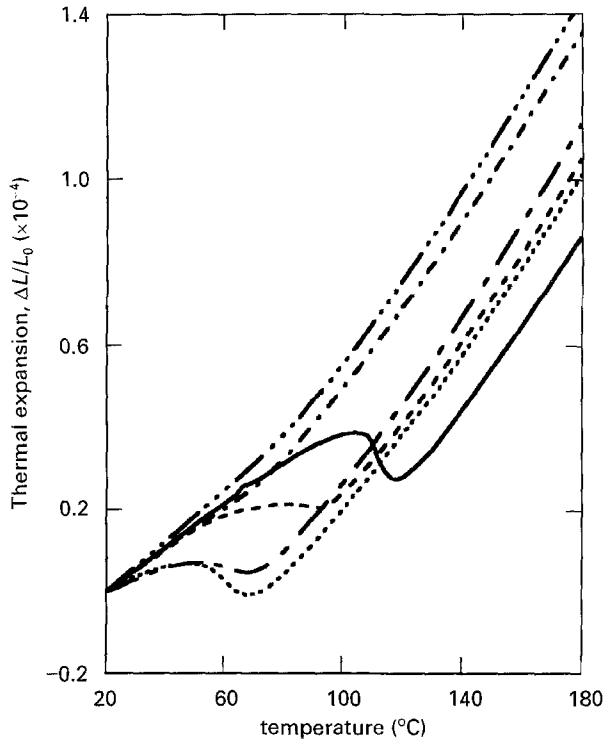

Figure 2 Variation of the linear thermal expansion with the SiC content for the $BaTiO_3$–SiC composites sintered at 1300 °C for 1 h in an argon atmosphere. SiC content (vol %): (—) 0, (– – –) 0.2, (- - -) 0.5, (—·—·—) 1, (–·–) 3, (–·····–) 5.

$BaTiO_3$-based composites with a low content of SiC. The crystal structure and the transformation behaviour are gradually modified by incorporating the SiC. First of all, the transformation in the low-temperature range, e.g. the tetragonal to orthorhombic transformation, seems to disappear at 1 vol % SiC. Furthermore, the cubic to tetragonal transformation is ambiguous and broadened, as mentioned in Fig. 2. In addition, there is no conspicuous change in the internal friction curve at 5 vol % SiC except for a slight and smooth change over the wide temperature range of 0–100 °C.

The grain-size change with respect to the SiC content is shown in Fig. 5 for specimens sintered at 1300 °C. The grain size drastically decreased with increasing SiC content. As expected from the results reported for other composite systems [14–16], it is apparent that SiC particulates strongly prevent grain-boundary migration and limit the grain growth. The average grain size decreased gradually from 1 or 2 μm (for the monolithic $BaTiO_3$) to less than 0.32 μm (for the composite with 10 vol % SiC) as the SiC content increased. These observed drastic reductions in the grain size with respect to the SiC content indicate that the SiC particulate is very effective in controlling the grain structure of $BaTiO_3$ ceramics.

Table III shows the relationship between the carrier density and SiC content for specimens sintered at 1300 °C. Both the monolithic $BaTiO_3$ and composites were n-type semiconductors. The carrier density gradually increased with SiC content. The carrier in the present specimens must be electrons from the oxygen vacancy produced by sintering in a reducing atmosphere.

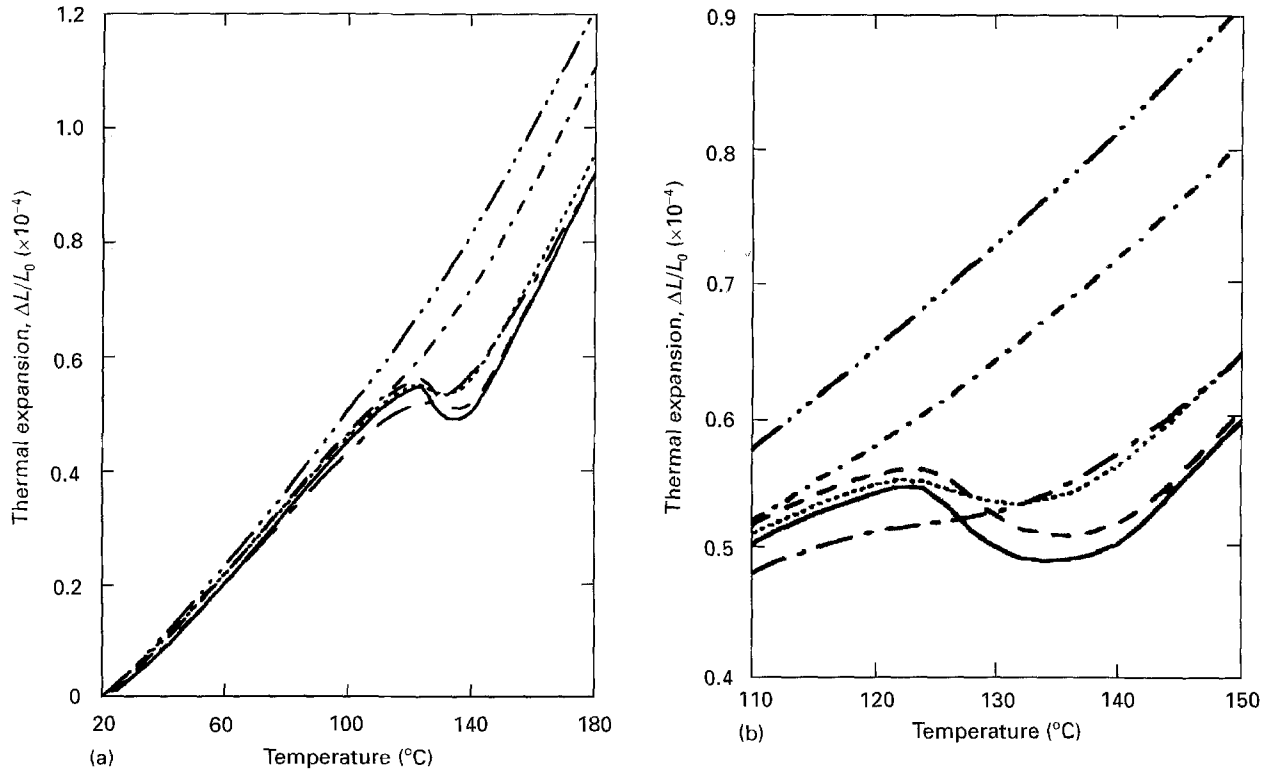

Figure 3 (a) Variation of the linear thermal expansion with SiC content for the $BaTiO_3$–SiC composites sintered at 1300 °C for 1 h in an argon atmosphere and subsequently oxidized at 1050 °C for 30 min in air. (b) Enlargement of an area of (a). For key, see Fig. 2.

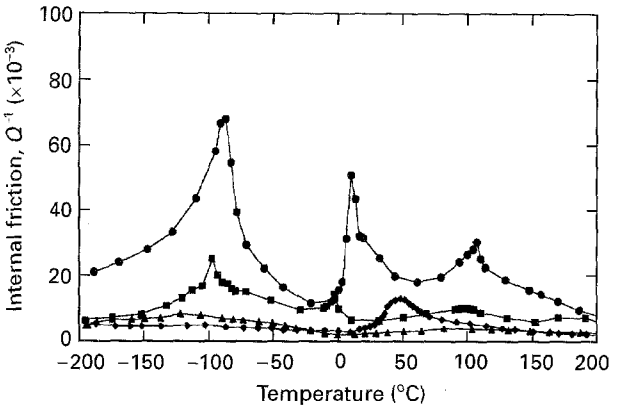

Figure 4 Temperature dependence of the internal friction for the monolithic $BaTiO_3$ and $BaTiO_3$–SiC composites sintered at 1300 °C. SiC content (vol %); (●) 0, (■) 0.2, (◆) 1, (▲) 5.

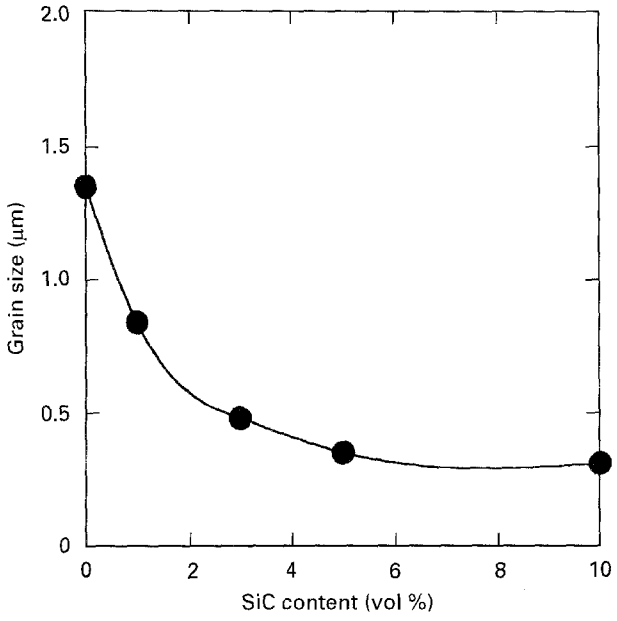

Figure 5 Grain-size variation with the SiC content for the $BaTiO_3$–SiC composites sintered at 1300 °C.

TABLE III Carrier concentration of monolithic $BaTiO_3$ and $BaTiO_3$-based composites with a different SiC content sintered at 1300 °C in argon

	SiC content (vol %)				
	0	0.2	1	3	5
Carrier concentration (10^{16} cm^3)	1.53	6.33	7.78	10.96	13.16

4. Discussion

From the X-ray diffraction analysis, thermal expansion analysis and internal friction measurements, it was found that the monolithic $BaTiO_3$ showed ferroelectric tetragonal phase regardless of the sintering temperature. The crystal structure, however, was gradually changed from the tetragonal to cubic as the SiC content increased. $BaTiO_3$-based composites with 3 and 5 vol % SiC, in particular, were pseudo-cubic. The transformation temperatures determined from internal friction curves, as well as the linear thermal expansion analysis, are summarized in Table IV. The results obtained from internal friction measurements are in good agreement with those from the linear thermal expansion analysis. As mentioned above, T_c decreased with increasing SiC content, and was finally ambiguous. In addition, the transformation at low temperatures completely disappeared on the addition of only 1 vol % SiC. This phenomenon is similar to the temperature-dependence behaviour of permittivity, ε_r, observed in the $Ba(Zr_x, Ti_{1-x})O_3$ system [21]. With increasing zirconium content, the three transformation points and the corresponding three ε_r maxima, move closer together and finally coalesce at about 10 mol % Zr addition ($x = 0.1$) into a single broad maximum. The strong increase and broadening of the ε_x maxima are commonly attributed to the overlapping of the three ε_r maxima at 10 mol % Zr addition. In the present study, it is suggested that the broadening of the internal friction curve observed for $BaTiO_3$–1 vol % SiC composite must be caused by the coexistence of the orthorhombic or rhombohedral phase, together with the pseudo-cubic. However, the exact crystal structure is not clear at present.

So far, the grain-size effect on the crystal structure and dielectric constant has been investigated extensively [22–25]. Of these investigations, it is well known that the crystal structure of $BaTiO_3$ with a grain size below 1 μm, changes from the ferroelectric tetragonal to paraelectric cubic phase. Hence, the grain-size dependence of the $\Delta L/L_0$ for $BaTiO_3$ can be illustrated as indicated in Fig. 6. The fine-grained $BaTiO_3$ exhibits no abrupt change in $\Delta L/L_0$ curves because the pseudo-cubic phase exists metastably even below the transformation temperature. In the present study, the same phenomenon also occurred for $BaTiO_3$-based composites with more than 1 vol % SiC as shown in Figs 1, 2 and 4. It is believed that this broadened transformation phenomenon must be caused by the reduction in grain size by incorporating the SiC particulate.

The change of T_c with increasing the SiC content can be explained by two factors: oxygen vacancies and the stress effect. According to Devries [20], it seems that T_c of $BaTiO_3$ ceramics fabricated by hot pressing in a reducing atmosphere, is modified by the chemical reduction, that is, oxygen vacancies. This phenomenon may be due to the suppression of the domain-structure development caused by the oxygen vacancies. It is evident, as shown in Table III, that the concentration of oxygen vacancies increased with increasing SiC content. Generally, if oxygen vacancies are produced in the $BaTiO_3$ lattice, some Ti^{4+} are reduced to Ti^{3+} in order to keep the charge neutrality. As the ionic radius of Ti^{3+} (0.076 nm) is larger than Ti^{4+} (0.068 nm) [26], deviation from the typical perovskite structure will occur. This phenomenon can be considered as the substitution of Ti^{4+} by Ti^{3+}. If many oxygen vacancies are produced in the $BaTiO_3$ lattice, considerable crystal structure change will be expected. On the other hand, it is believed that the increase in the carrier density is caused by the

TABLE IV Transformation temperature of monolithic $BaTiO_3$ and $BaTiO_3$-based composites with particulate SiC determined by the internal friction and thermal expansion measurement

SiC content (vol %)	Phase transformation temperature (°C)			
	Cubic–tetragonal		Tetragonal–monoclinic	Monoclinic–rhombohedral
	IF[a]	TE[b]		
0	108.0	120	10.3	− 86.3
0.2	97.8	100	− 2.8	− 92.9
1	51.3	58	No trans.[c]	No trans.
3	0–100	30–60	–	–
5	0–100	30–60	No trans.	No trans.

[a] IF, internal friction measurement.
[b] TE, linear thermal expansion measurement.
[c] No trans, no transformation (no shaped peak of internal friction curve in Fig. 5).

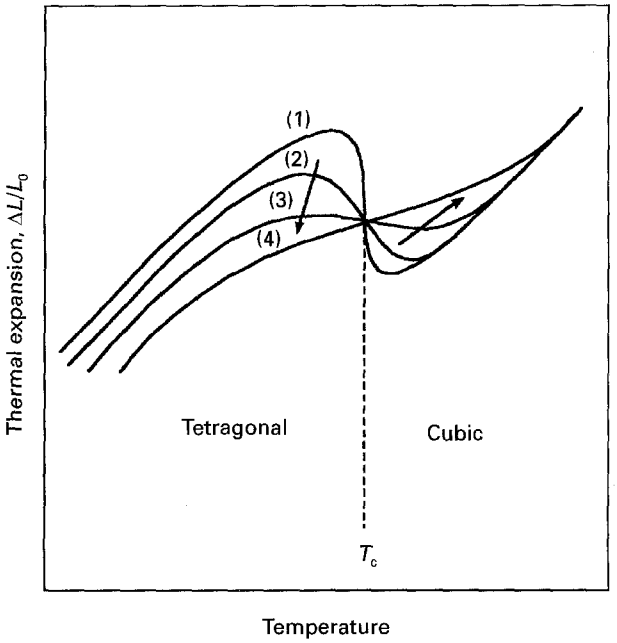

Figure 6 Schematic diagram showing the variation of tetragonal to cubic transformation behaviour for $BaTiO_3$–SiC composites with different grain sizes; (1) > (2) > (3) > (4).

grain-size decrease owing to the incorporation of the SiC particulate. It should be recalled that the rate-determining path of the diffusivity of an oxygen vacancy is lattice diffusion, not grain-boundary diffusion. The observed carrier density increase, can thus be explained by shortening the diffusion distance of an oxygen vacancy.

Another possible factor influencing the phase transformation behaviour is the residual stress, which was developed during the cooling process from the fabrication temperature. According to Selsing [27], the residual stress is developed in the sintered body owing to the thermal expansion coefficient difference between the matrix and the dispersed particle as a secondary phase during the cooling process. The residual stress is expressed as

$$\sigma = \Delta\alpha\,\Delta T/\{(1 + n_m)[2E_m + (1 - 2n_d)]E_d\} \quad (1)$$

where $\Delta\alpha$ is the difference in thermal expansion coefficient between the matrix and the dispersive phase, ΔT is the cooling range, E_d, n_m and E_d, n_d are Young's moduli and Poisson's ratios of the matrix and dispersive phase, respectively. As the thermal expansion mismatch between $BaTiO_3$ and SiC ($14 \times 10^{-6}\,°C^{-1}$ for $BaTiO_3$ and $4 \times 10^{-6}\,°C^{-1}$ for β-SiC) is large enough, it is suggested that a considerable amount of residual stress is developed around SiC particulates incorporated within $BaTiO_3$ grains. By substituting the Young's moduli and Poisson's ratios of $BaTiO_3$ and SiC into Equation 1, the residual stress developed around the SiC particulate can be calculated to be ~1.2 GPa tensile stress to the tangent and ~2.4 GPa compressive stress to the radius of the dispersive SiC particulate. Although this calculation is approximate, it is suggested that the matrix $BaTiO_3$ grain experiences a complex stress system and it results in T_c change of the $BaTiO_3$–SiC composites.

According to TEM observation for Al_2O_3–SiC nanocomposites in which nanosized SiC was mainly dispersed within the matrix grains by Niihara *et al.* [28, 29], dislocation networks were formed around the SiC particulate owing to the residual thermal stress generated during the cooling processes from the fabrication temperature. Fig. 7 shows the formation of dislocation networks observed for $BaTiO_3$–5 vol % SiC composite. It is believed that these observed dislocation networks are formed due to the pile-up of dislocations generated by residual stresses and their pinning by the nanosized SiC. The formation of dislocation networks indicates that $BaTiO_3$ grains around the SiC particulate are subjected to highly localized stresses.

Fig. 8 shows typical transmission electron micrographs of $BaTiO_3$ and $BaTiO_3$–1 vol % SiC composite. For the monolithic $BaTiO_3$ the polarization domain structures can be clearly seen. Dark and bright fringes are observed, indicating that the lattice periodicity is changed and the orientation of polarization to each other is 90°, as pointed out by other reports [30, 31]. However, there are no domain structures for the grains in which the SiC particulates are dispersed, as can be seen in Fig. 7b. This phenomenon must be caused by the residual stress developed around SiC particulates, as mentioned above.

The decrease in T_c with increasing the SiC content is explained by taking account of the strains introduced into the lattice at the paraelectric cubic to

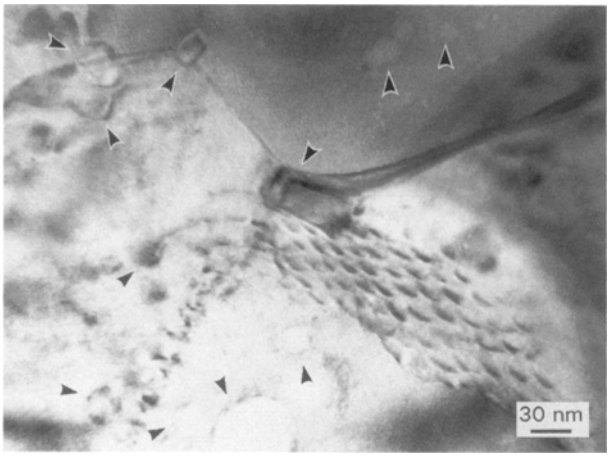

Figure 7 The development of dislocation networks owing to the residual stresses within $BaTiO_3$ grains for the $BaTiO_3$–5 vol % SiC composite. Arrows indicate the intragranular SiC.

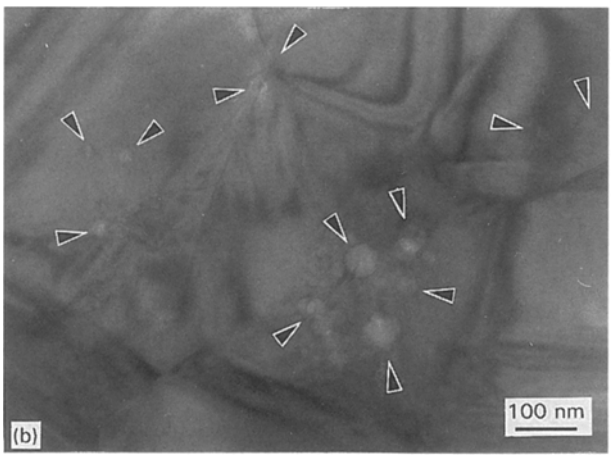

Figure 8 Transmission electron micrographs of (a) the monolithic $BaTiO_3$ and (b) $BaTiO_3$–SiC composite with 1 vol % SiC, sintered at 1300 °C. Arrows indicate the intragranular SiC as in Fig. 7b.

ferroelectric tetragonal phase transformation. As this transformation involves the volume expansion, the external stresses generated in grains result in a depression of the transformation and therefore a decrease in T_c [22, 31, 32]. Consequently, it is concluded that the SiC incorporated within $BaTiO_3$ grains influences not only the developing domain structure, but also the transformation behaviour by the highly localized thermal stresses within and/or around the SiC particulates arising from the thermal expansion mismatch between $BaTiO_3$ and SiC. However, this is not yet clear and further investigation is required to understand the effect of the SiC particulate incorporated within $BaTiO_3$ on the domain structure.

5. Conclusion

$BaTiO_3$-based composites, in which nanosized SiC particulates were mainly dispersed within the matrix grains, were successfully fabricated by hot-pressing the $BaTiO_3$ and SiC powder mixtures in an argon atmosphere. Their crystal structure and phase transformation behaviour were investigated by X-ray diffraction analysis, linear thermal expansion analysis and internal friction measurement. The crystal structure at room temperature gradually changed from tetragonal to cubic as the SiC content increased. For $BaTiO_3$-based composite with over 3 vol % SiC, the crystal structure was pseudo-cubic. The Curie temperature, T_c, was lowered with increasing SiC content and became ambiguous, and finally the diffused phase transformation (DPT) was observed as the SiC content increased to 3 vol %. Moreover, the low-temperature transformation also disappeared completely above 1 vol % SiC. These results are associated with the existence of oxygen vacancies produced by sintering in a reducing atmosphere. From TEM observations it is evident that $BaTiO_3$ experiences complex residual stress systems, which are generated from the thermal expansion mismatch between the matrix and SiC particulate. These residual stresses result in a decrease in T_c and crystal structure variation. The SiC particulates dispersed within the matrix grains also influence the development of domain structure.

References

1. Y. M. CHIANG and T. TAKAJI, *J. Am. Ceram. Soc.* **73** (1990) 3286.
2. W. HEYWANG, *Solid State Electron.* **31** (1961) 51.
3. G. H. JONKER, *ibid.* **7** (1964) 895.
4. H. L. HSIGH and T. T. FANG, *J. Am. Ceram. Soc.* **73** (1990) 1566.
5. S. K. NAG and D. C. AGRAWAL, *J. Mater. Sci.* **27** (1992) 4125.
6. O. SABURI, *J. Am. Ceram. Soc.* **44** (1961) 54.
7. C. J. TING, C. J. PENG, H. Y. LU and S. T. WU, *ibid.* **73** (1990) 329.
8. H. IHRIG, *ibid.* **64** (1981) 617.
9. H. F. CHENG, T. F. LIN, C. T. HU and I. N. LIN, *ibid.* **76** (1993) 827.
10. S. K. CHIANG, W. E. LEE and D. W. READEY, *Am. Ceram. Soc. Bull.* **66** (1987) 1230.
11. T. R. ARMSTRONG and R. C. BUCHANAU, *J. Am. Ceram. Soc.* **73** (1990) 1268.
12. H. EMOTO and J. HOJO, *J. Ceram. Soc. Jpn* **100** (1992) 555.
13. B. MALIC, M. KOSEC and T. KOSMAC, *Ferroelectrics* **129** (1992) 147.
14. A. NAKAHIRA and K. NIIHARA, *J. Ceram. Soc. Jpn* **100** (1992) 448.
15. I. THOMPON and V. D. KRSTIC, *J. Mater. Sci.* **27** (1992) 5765.
16. E. D. CASE, J. R. SMYTH and V. MONTHEI, *J. Am. Ceram. Soc.* **64** (1981) C-24.

17. P. R. VAYA, J. MAJHI, B. S. V. GOPALAM and C. DATTATREYAN, *Phys. Status Solidi A* **87** (1985) 341.
18. Z. M. HANAFI, F. M. ISMAIL, F. F. HAMMAD and S. A. NASSER, *J. Mater. Sci* **27** (1992) 3988.
19. H. AREND and L. KIHLBORG, *J. Am. Ceram. Soc.* **52** (1969) 63.
20. R. C. DEVRIES, *ibid.* **43** (1960) 226.
21. D. HENNINGS and A. SCHNELL, *ibid.* **65** (1982) 539.
22. W. R. BUESSEM, L. E. CROSS and A. K. CTOSWAMI, *ibid.* **49** (1966) 33.
23. S. KAHN, *ibid.* **54** (1971) 452.
24. A. J. BELL and A. J. MOULSON, *Ferroelectrics* **54** (1984) 147.
25. K. ISHIKAWA, K. YOSHIKAWA and N. OKADA, *Phys. Rev. B* **37** (1988) 5852.
26. R. D. SHANNON and C. T. PREWITT, *Acta Crystallogr.* **B25** (1969) 925.
27. J. SELSING, *J. Am. Ceram. Soc.* **79** (1961) 419.
28. K. NIIHARA, T. HIRANO, A. NAKAHIRA, K. OJIMA, K. IZAKI and T. KAWAKAMI, in "Proceedings of MRS International on Advanced Material", Vol. 5, edited by M. Doyama, S. Somiya and R. P. H. Chang (Materials Reserach Society, Pittsburgh, PA, 1989) p. 107.
29. K. NIIHARA, A. NAKAHIRA, T. UCHIYAMA and T. HIRAI, in "Fracture Mechanics of Ceramics", Vol. 4, edited by R. C. Bradt, A. G. Evans, D. P. H. Hasselman and F. F. Lange (Plenum Press, New York, 1985) p. 103.
30. K. KOUMOTO, H. TAGAWA, T. NAKANO, S. TAKEDA and H. YANAGIDA, *Jpn. J. Appl. Phys.* **23** (1984) L305.
31. G. A. SAMURA, *Phys. Rev.* **151** (1966) 378.
32. D. L. DECKER and Y. X. ZHAO, *Phys. Rev. B* **39** (1989) 2432.

Received 1 December 1994
and accepted 13 February 1995